PERGAMON

Computers and Structures 69 (1998) 719–738

Computers & Structures

A review of homogenization and topology opimization II—analytical and numerical solution of homogenization equations

B. Hassani, E. Hinton *

Department of Civil Engineering, University of Wales, Swansea, Singleton Park, Swansea, SA2 8PP, U.K.

Received 28 January 1997; accepted 28 April 1998

Abstract

This is the second part of a three-paper review of homogenization and topology optimization. In the first paper, we focused on the theory and derivation of the homogenization equations. In this paper, motives for using the homogenization theory for topological structural optimization are briefly explained. Different material models are described and the analytical solution of the homogenization equations for the so called "rank laminate composites" is presented. The finite element formulation is explained for the material model, based on a miscrostructure consisting of an isotropic material with rectangular voids. Using the periodicity assumption, the boundary conditions are derived and the homogenization equations are solved, and the results to be used in topology optimization are presented. The third paper deals with the use of homogenization for structural topology optimization by using optimality criteria methods.

1. Introduction

Topological structural optimization has the complex features of both size and shaope optimization problems. One of the drawbacks of conventional shape optimization by the boundary variation method is that final designs are topologically equivalent to the initial ones. Normally these techniques require several finite element re-meshings in the optimization process. Furthermore, the difficulty of changing the topology during the scheme increases the complexity of the problem. In topological structural optimization we need to be able to create new holes, and this cannot be achieved in the boundary variation method. In addition, unlike the conventional shape optimization methods where the design boundary can be described by a set of simple geometrical segments (i.e. lines, circular arcs, elliptic arcs and splines), it is not easy to define the structural topology optimization problem by using a finite number of parameters.

Studying the nature of the topological structural shape optimization problem suggests a specific and different sort of parameterization from the outset: that is the natural formulation of an infinite number of holes of varying size, which implies the existence of a special microstructure. It has already been proven that in some cases, having a finite number of design variables does not lead to the optimum solution. For example, in the problem of thickness optimization of a linearly elastic plate, with mean compliance considered as the objective function, Cheng and Olhoff [1,2] demonstrated that it is not realistic to define this problem by using a fixed, finite number of parameters and basic functions, as the true optimum problem consists of many discrete ribs of various sizes. This problem has also been studied by Lurie et al. [3] using the theory of *G*-closure. They concluded that it is necessary to introduce the relaxed form of the state equation by using an orthotropic plate that may possess a microstructure. This was also confirmed by Rozvany et al. [4] and Ong et al. Szeto [5]. Kohn and Strang [6] established that in the context of plastic design for torsion of a cross-section within a square area, the generalized

* Corresponding author.

0045-7949/98/$ - see front matter
PII: S0045-7949(98)00132-1

shape optimization (i.e. both shape and topology) may yield three types of regions: solid, empty and porous, where the pourous regions comprise some material with infinitesimal cavities, see Ref. [7]. Also, by introducing a microstructure to the material model [8], they could obtain a well-posed, relaxed formulation for a two-dimensional (2D) heat conduction problem. The main advantage of this relaxed formulation is that the solution with the finite element method, is no longer mesh-dependent.

Structural shape optimization, in general, can be thought of as the determination of the optimal spatial material distribution. In other words, for a given set of loads and boundary conditions, the problem is how to redistribute the material in order to minimize the objective function, for example, the mean compliance. Therefore, the general shape optimization problem can be considered as a point-wise material/no material which does not need to be represented by the shape parameters or basic shape functions. However, implementation of this on–off approach to an optimization problem requires the use of discrete optimization algorithms. Such an approach would be unstable, unless composite materials were introduced. "In general, existence of solutions cannot be expected unless the problem is turned into a material distribution one, usin composite materials" (Bendsøe [9]).

Intoducing a material density function by considering a composite consisting of an infinite number of infinitely small holes which are periodically distributed, the complex nature of the structural topological optimization problem can be converted to a sizing problem. In fact, using the idea of using a cellular body with a periodic microstructure, moves the on–off nature of the problem from the macroscopic scale to the microscopic scale [9]. In mathematical terms the introduction of microstructures corresponds to a relaxation of the variational problem that can be established for the optimization problem [8, 10].

There are many ways to introduce the above mentioned microstructures and these can be divided into two categories: rank laminate composite methods and microcells with internal voids that will be defined in the next section. The theory of homogenization is used to determine the macroscopic mechnical properties of these materials. In the case of rank materials the homogenization equation can be solved analytically, but for the voided microcells it usually has to be solved by numerical methods such as finite elements.

In practice, after choosing the reference domain and finite element discretization, it is assumed that each element consists of a cellular material with a specific microstructure, and the geometrical parameters of these microstructures are the design variables of the optimization problem. It is noted that the problem is solved in a fixed domain, so that the finite element model used in the analysis does not need to be altered during the optimization algorithm.

An alternative direct approach to the discrete optimization problem of material distribution exists, which substitutes the on–off character of the problem by a suitable differentiable approximation called an "artificial density function". These are usually referrd to as artificial materials. In this paper, microcells with rectangular voids, the so-called rank-2 materials, and the artificial materials are considered.

2. Material Models

As mentioned in the introduction, the main idea of solving a class of shape optimization problems involving topology is to introduce an "infinite" number of microscale voids to form a porous medium. The optimization problem is defined in such a way that the geometry parameters of these voids are the design variables. If a portion of the medium consists only of voids, material is not placed over that area. On the other hand, if there is no porosity at some portion, a solid structure needs to be placed at that location. Some common ways of creating these microstructures are now introduced.

2.1. Rectangular microscale voids

In choosing the microstructure, one of the important features that should be considered is that it should allow the density of material to cover the whole range of values from zero (void) to one (solid). For example, circular holes (spherical in 3D) do not allow this, because they cannot provide a complete void. In addition, they should fit the periodicity assumption and their geometry should be defined by very few parameters (as these are the design variables of the optimization algorithm). Square cells with centrally-placed rectangular holes are one of the simplest means of achieving this objective (Fig. 1). In 3D space this microcell will be a cubic cell with a rectangular parallel-poped hole in it.

Another possibility, for example, is the generalized ellipsoid [11] defined by:

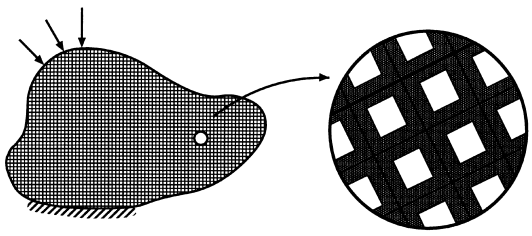

Fig. 1. Microcells with rectangular holes.

$$\left(\frac{y_1}{a}\right)^m+\left(\frac{y_2}{b}\right)^m+\left(\frac{y_3}{c}\right)^m=1,$$

where a, b and c are the principal radii of the ellipsoid and m is a large number. If the dimension of the square cell is denoted by ϵ which is a very small positive number, then the size of the hole will be ϵa and ϵb. Fig. 2 illustrates this unit cell in the microscopic coordinates. Using this model, the area occupied by the solid material is given by:

$$\Omega_s=\int_\Omega (1-ab)\mathrm{d}\Omega, \tag{1}$$

where $0\le a\le 1$, $0\le b\le 1$, Ω is the design domain and Ω_s denotes the solid part of it.

In general, the microscale perforations in the cellular body, with respect to the coordinate axes, can have different orientations. Since this orientation θ will affect the properties of the elastic consitutive matrix, it has to be taken into account in the formulation. As each point $\mathbf{x}\in\Omega$ has its own a, b and θ values, these parameters can be considered as distributed functions of the position vector $\mathbf{x}$ and these are the design variables of the relaxed optimization problem. According to the theory, the functions $a=a(\mathbf{x})$, $b=b(\mathbf{x})$ and $\theta=\theta(\mathbf{x})$ are assumed to be smooth enough, for example, $a,b,\theta,\in H^1(\Omega)$. On the other hand, to be able to construct the optimization formulation, these functions have to be represented by discrete approximations, otherwise there will be an infinite number of design variables. In practice, these functions are approximated by constant functions in each finite element of the discretized model of the design domain. Thus, a constant microstructure is assumed inside each element and the homogenized elasticity matrix will, therefore, also be constant in each finite element. Thus, if the design domain Ω is decomposed into N finite elements, then we will have $3N$ design variables, [i.e. (a_i,b_i,θ_i) $i=1,2,\ldots,N$].

Assuming that the solid part of the microstructure is an isotropic material, because of the rectangular perforations the cellular body becomes an orthotropic one. For the 2D (plane stress/strain) elastic problem the constitutive law will be:

$$\begin{Bmatrix}\sigma_{11}\\ \sigma_{22}\\ \sigma_{12}\end{Bmatrix}=\begin{bmatrix}D_{11} & D_{12} & 0\\ D_{12} & D_{22} & 0\\ 0 & 0 & D_{66}\end{bmatrix}\begin{Bmatrix}\epsilon_{11}\\ \epsilon_{22}\\ 2\epsilon_{12}\end{Bmatrix}, \tag{2}$$

where σ_{ij} $(i,j=1,2)$, are the stresses and ϵ_{ij} denotes the strains. D_{ij} are the elements of the reduced stiffness matrix of material.

It is noted that for the cellular material the elements of the matrix of elastic moduli $\mathbf{D}$ are functions of a,b and θ, so that

$$\mathbf{D}=\mathbf{D}(a,b,\theta). \tag{3}$$

The dependency on a and b is calculated by the asymptotic homogenization theory and one can find the dependency on θ by using the well-known frame rotation formula:

$$\mathbf{D}=\mathbf{R}(\theta)^{\mathrm{T}}\mathbf{D}^{\mathrm{H}}(a,b)\mathbf{R}(\theta), \tag{4}$$

where $\mathbf{R}$ is the matrix of rotation. This issue will be discussed later. We also note that the density function ρ is a function of a and b:

$$\rho=\rho(a,b)=(1-ab)\rho_s, \tag{5}$$

where ρ_s is the density of the solid. Similarly, for inertia body forces we can write

$$\mathbf{f}=\mathbf{f}(a,b)=\rho_s(1-ab)\boldsymbol{\gamma}, \tag{6}$$

where $\boldsymbol{\gamma}$ is a known vector.

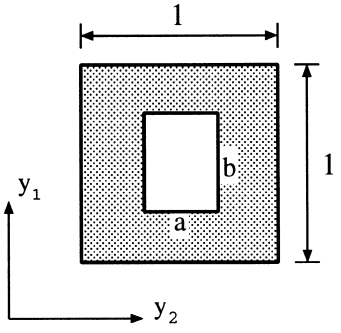

Fig. 2. Unit cell with rectangular hole in microscopic coordintes.

2.2. Ranked layered material cells

Layered materials are another type of microstructure that can be applied in order to produce a relaxed form of the topoligical structural optimization problem. Each cell of this periodic microstructure is construced from layers of different materials and voids. The so-called rank-1 material is constructed of alternating layers of solid materials and voids. In practice, to avoid singularity in the stiffness matrix of the structue, instead of voids a very soft (flexible) material is used. The relative densities of the solid and soft layers are, respectively, denoted by γ and $1-\gamma$, see Fig. 3.

This material can be used to construct the higher ranks of layered composites. For example, the rank-2 composite is constructed by repeating layers of the solid and the rank-1 composite with relative densities of μ and $1-\mu$, respectively. The direction of the layers of different ranks are orthogonal to each other. The characteristic width of these layers are of different orders. In other words, the real width of a unit layer

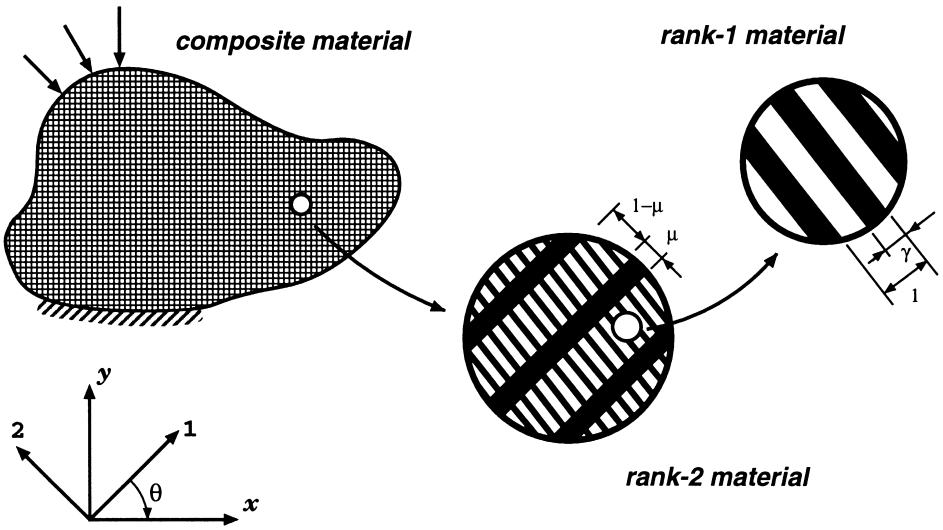

Fig. 3. Construction of the rank-2 layered material.

(cell) of rank-1 material in comparison to the real width of rank-2 material is a very small number.

Recent studies on the effective material properties of composite mixtures of two different materials have shown that in plane elasticity problems, the rank-2 composites yield the stiffest material [12–15].

As for the case of microstructures with rectangular voids, the elements of the matrix of elasticity coefficients for rank-2 materials, are functions of three parameters: γ, μ and the orientation angle θ; (see Fig. 3) so that:

$$\mathbf{D} = \mathbf{D}(\gamma, \mu, \theta). \tag{7}$$

The volume occupied by the solid (neglecting the very soft material) is

$$\Omega_s = \int_\Omega (\mu + \gamma - \mu\gamma) \mathrm{d}\Omega, \tag{8}$$

and the density of the composite can be written as

$$\rho = \rho(\gamma, \mu) = (\gamma + \mu - \gamma\mu)\rho_s, \tag{9}$$

where ρ_s is the density of solid and $0 \leq \gamma$ and $\mu \leq 1$. It is noted that by changing the values of γ and μ it is possible to cover the complete range of cell relative densities from zero (void) to one (solid).

Olhoff et al. [16] and Thomsen [17] have used a bi-material rank-2 composite for the topology optimization problem. This model makes it possible to generate typical sandwich structures. The rank-1 material is constructed from two isotropic materials: one with a relatively large stiffness, and one with a very soft material which represents the voids. The rank-2 material is constructed by using the stiffest material in one direction and the rank-1 composite layers in the perpendicular direction. Fig. 4 illustrates the different levels of construction. At the first level shown in Fig. 4(a), the composite is modelled by using isotropic stiff materials, S_1 and S_2, with concentrations given by γ_1 and $1-\gamma_1$ respectively. In the second level, the above mentioned material is compounded with a very soft material (representing the void) with relative concentrations of γ_2 and $1-\gamma_2$, as shown in Fig. 4(b). At

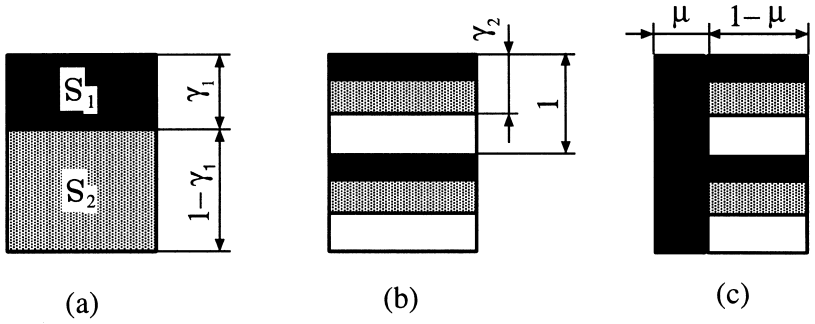

Fig. 4. Construction of a rank-2 bi-material composite.

the third level, the rank-2 composite is constructed by using material S_1 (the stiffest one) an the composite in Fig. 4(b), with relative concentrations μ and $1-\mu$, respectively [Fig. 4(c)]. In this case, the density at each point of the composite is a function γ_1, γ_2 and μ and the densities of the stiff materials ρ_{s_1} and ρ_{s_2}, and has the form:

$$\rho = \mu\rho_{s_1} + (1-\mu)\gamma_1\gamma_2\rho_{s_1} + (1-\mu)(1-\gamma_1)\gamma_2\rho_{s_1}. \quad (10)$$

For the volume of the materials we can write:

$$\Omega_{s_1} = \int_\Omega [\mu + (1-\mu)\gamma_1\gamma_2]\mathrm{d}\Omega$$

and

$$\Omega_{s_2} = \int_\Omega [(1-\mu)(1-\gamma_1)\gamma_2]\mathrm{d}\Omega. \quad (11)$$

It is noted that the elements of the constitutive matrix in this case are functions of γ_1, γ_2, μ and θ, so that

$$\mathbf{D} = \mathbf{D}(\gamma_1, \gamma_2, \mu, \theta), \quad (12)$$

where θ is the angle of orientation of layers with respect to the main coordinates. By using this model for structural topology optimization in every element we have four design variables.

2.3. Artificial materials

By considering the general shape and topology optimization of structures as a material distribution problem, the structure can be described by a discrete function χ, defined at each point $\mathbf{x}$ as:

$$\chi(\mathbf{x}) = \begin{cases} 1 & \text{if} \quad \mathbf{x} \in \Omega_s \quad \text{material} \\ 0 & \text{if} \quad \mathbf{x} \in \Omega\backslash\Omega_s \quad \text{no material.} \end{cases} \quad (13)$$

Assuming isotropy for the solid part of the structure, we can write

$$\rho(\mathbf{x}) = \chi(\mathbf{x})\rho^0, \quad (14)$$

and

$$\mathbf{D}(\mathbf{x}) = \chi(\mathbf{x})\mathbf{D}^0, \quad (15)$$

where ρ^0 and $\mathbf{D}^0$ are, respectively, the density and elasticity matrix of the homogeneous solid.

For the numerical solution of the optimization problem, the indicator function $\chi(\mathbf{x})$ has to be discretized and this yields an integer programming problem, where $\chi^*(\mathbf{x}^e)$ within each element e are the design variables. However, this formulation, apart from being expensive, is not well posed [8]. This is partly because of strong dependency of the optimization results on the chosen discretization and, furthermore, the integer formulation comprises many artificial local minima [18].

The very easy way to relax the problem is to replace the discrete value parameter $\chi(\mathbf{x})$ with a continuous one $\xi(\mathbf{x})$, so that

$$\rho(\mathbf{x}) = \xi(\mathbf{x})\rho^0 \quad (16)$$

and

$$\mathbf{D}(\mathbf{x}) = \xi(\mathbf{x})\mathbf{D}^0, \quad (17)$$

where $0 \le \xi(\mathbf{x}) \le 1$ and $\mathbf{x} \in \Omega$. Note that according to Eq. (16) the volume of material is obtained by:

$$Vol = \int_\Omega \xi(\mathbf{x})\mathrm{d}\Omega. \quad (18)$$

Although Eqs. (16) and (17) yield a relaxed optimization algorithm, it results in some porous areas in the optimum structure. From an engineering point of view, it is more practical to obtain a solution which only consists of solid and void regions. Hence, it may be desirable to suppress the porous areas by penalizing the intermediate values for $\xi(\mathbf{x})$. This idea is explained by Rozvany et al. by introducing the fabrication cost of voids [7, 19, 20]. Also, it can easily be provided by changing Eq. (17) to the form

$$\mathbf{D}(\mathbf{x}) = \xi(\mathbf{x})^\mu\mathbf{D}^0, \quad (19)$$

where $\mu > 1$ and is usually between 3 and 9 [9, 21, 22] and the larger μ value results in fewer perforated regions. Note that as the volume of the structure is linear in ξ, the intermediate values give a little stiffness at an undesirable cost [9].

The artificial density function ξ can also be related to some geometrical parameters to create some sort of artificial microstructures. For example, to make analogy to the idea of a cellular body consisting of unit cells with rectangular holes, $\xi(\mathbf{x})$ may be considered as:

$$\xi(\mathbf{x}) = 1 - a(\mathbf{x})b(\mathbf{x}).$$

Assuming isotropy for the material, the matrix of the artificial elasticity constants of a plane stress problem ca be written as [11]:

$$\mathbf{D}^{\mathrm{H}} = \frac{(1-ab)^\mu E}{(1-v^2)}\begin{bmatrix} 1 & v & 0 \\ v & 1 & 0 \\ 0 & 0 & (1-v)/2 \end{bmatrix}. \quad (20)$$

This idea can also be extended to an orthotropic material model which relieves the dependency of results on finite element meshes [18, 23]. Thus, $\mathbf{D}^{\mathrm{H}}$ has the form:

$$\mathbf{D}^{\mathrm{H}} = \frac{1}{(1-v^2)}\begin{bmatrix} E_1 & v\sqrt{E_1E_2} & 0 \\ v\sqrt{E_1E_2} & E_2 & 0 \\ 0 & 0 & G \end{bmatrix}, \quad (21)$$

where $G = (1-v)\sqrt{E_1E_2}/2$ and $\xi = \xi_1 + \xi_2 - \xi_1\xi_2$.

ξ_1 and ξ_2 are the independent artificial density functions and $E_1 = E^0\xi_1^\mu$, $E_2 = E^0\xi_2^\mu$ and $\rho = \xi\rho^0$. E^0, v and ρ^0 are the modulus of elasticity, Poisson's ratio and density of material, respectively.

There is some controversy about the verification of using the artificial material model in structural topology optimization problems. Bendsøe [9] believes that "the scheme is very dependent on the mesh and it is impossible to given any physical meaning to intermediate values of ξ". Rozvany et al. [24] has questioned the above statement: "The authors of this paper do not find, however, that the results are highly mesh dependent, nor that a physical interpretation of this model is impossible".

3. Analytical Solution of the Homogenization Equation For Rank Laminate Composites

Recalling from the homogenization theory (see Section 6 of Ref. [25]) in the case of traction forces inside the microcells of the cellular body, which is the case used in topological structural optimization, the governing equations are:

$$\int_{\mathbf{Y}} E_{ijpq}\frac{\partial\chi_p^{kl}}{\partial y_q}\frac{\partial v_i(\mathbf{y})}{\partial y_j}\mathrm{d}\,Y = \int_{\mathbf{Y}} E_{ijpq}\frac{\partial v_i(\mathbf{y})}{\partial y_j}\mathrm{d}\,Y, \quad \forall \mathbf{v}\in\mathbf{V}_{\mathbf{y}}, \tag{22}$$

$$E^{\mathrm{H}}_{ijkl}(\mathbf{x}) = \frac{1}{|Y|}\int_{\mathbf{Y}}\left(E_{ijkl} - E_{ijpq}\frac{\partial\chi_p^{kl}}{\partial y_q}\right)\mathrm{d}\,Y. \tag{23}$$

The microscopic characteristic displacement field χ^{kl} is the **Y**-periodic solution of Eq. (22) and it is used in Eq. (23) to find the effective elasticity coefficients. Eqs. (22) and (23) with different values of k and l provide enough equation to find the elements of the homogenized matrix $\mathbf{D}^{\mathrm{H}}$. For 2D problems (I, j, k, l, p, q = 1,2) it would be sufficient to solve them for the cases (**a**: $k = l = 1$), (**b**: $k = l = 2$) and (**c**: $k = 1$, $l = 2$).

case a: $k = 1$, $l = 1$

Expanding Eq. (22) and assuming orthotropicity for the material and removing terms with zero coefficients, we obtain:

$$\begin{aligned}&\int_Y\Bigg[\left(E_{1111}\frac{\partial\chi_1^{11}}{\partial y_1} + E_{1122}\frac{\partial\chi_2^{11}}{\partial y_2}\right)\frac{\partial v_1}{\partial y_1}\\ &\quad + E_{1212}\left(\frac{\partial\chi_1^{11}}{\partial y_2} + \frac{\partial\chi_1^{11}}{\partial y_2} + \frac{\partial\chi_2^{11}}{\partial y_1}\right)\left(\frac{\partial v_1}{\partial y_2} + \frac{\partial v_2}{\partial y_1}\right)\\ &\quad + \left(E_{1122}\frac{\partial\chi_1^{11}}{\partial y_1} + E_{2222}\frac{\partial\chi_2^{11}}{\partial y_2}\right)\frac{\partial v_2}{\partial y_2}\Bigg]\mathrm{d}\,Y\\ &= \int_Y\left(E_{1111}\frac{\partial v_1}{\partial y_1}E_{1122}\frac{\partial v_2}{\partial y_2}\right)\mathrm{d}\,Y,\end{aligned} \tag{24}$$

and considering the case $i = j = 1$, from Eq. (23) it follows that:

$$E^{\mathrm{H}}_{1111} = \frac{1}{|Y|}\int_Y\left(E_{1111} - E_{1111}\frac{\partial\chi_1^{11}}{\partial y_1} - E_{1122}\frac{\partial\chi_2^{11}}{\partial y_2}\right)\mathrm{d}\,Y, \tag{25}$$

and if $i = j = 2$, Eq. (23) we obtain:

$$E^{\mathrm{H}}_{2211} = \frac{1}{|Y|}\int_Y\left(E_{2211} - E_{2211}\frac{\partial\chi_1^{11}}{\partial y_1} - E_{2222}\frac{\partial\chi_2^{11}}{\partial y_2}\right)\mathrm{d}\,Y, \tag{26}$$

case b: $k = 2$, $l = 2$

Following the same procedure as above, Eq. (22) results in:

$$\begin{aligned}&\int_Y\Bigg[\left(E_{1111}\frac{\partial\chi_1^{22}}{\partial y_1} + E_{1122}\frac{\partial\chi_2^{22}}{\partial y_2}\right)\frac{\partial v_1}{\partial y_1}\\ &\quad + E_{1212}\left(\frac{\partial\chi_1^{22}}{\partial y_2} + \frac{\partial\chi_2^{22}}{\partial y_1}\right)\left(\frac{\partial v_1}{\partial y_2} + \frac{\partial v_2}{\partial y_1}\right)\\ &\quad + \left(E_{2211}\frac{\partial\chi_1^{22}}{\partial y_1} + E_{2222}\frac{\partial\chi_2^{22}}{\partial y_2}\right)\frac{\partial v_2}{\partial y_2}\Bigg]\mathrm{d}\,Y\\ &= \int_Y\left(E_{1122}\frac{\partial v_1}{\partial y_1} + E_{2222}\frac{\partial v_2}{\partial y_2}\right)\mathrm{d}\,Y.\end{aligned} \tag{27}$$

If $i = j = 1$, Eq. (23) becomes:

$$E^{\mathrm{H}}_{1122} = \frac{1}{|Y|}\int_Y\left(E_{1122} - E_{1111}\frac{\partial\chi_1^{22}}{\partial y_1} - E_{1122}\frac{\partial\chi_2^{22}}{\partial y_2}\right)\mathrm{d}\,Y, \tag{28}$$

and for $i = j = 2$, Eq. (23) yields:

$$E^{\mathrm{H}}_{2222} = \frac{1}{|Y|}\int_Y\left(E_{2222} - E_{2211}\frac{\partial\chi_1^{22}}{\partial y_1} - E_{2222}\frac{\partial\chi_2^{22}}{\partial y_2}\right)\mathrm{d}\,Y. \tag{29}$$

case c: $k = 1$, $l = 2$

Similarly, in this case, from Eq. (22) we obtain:

$$\begin{aligned}&\int_Y\Bigg[\left(E_{1111}\frac{\partial\chi_1^{12}}{\partial y_1} + E_{1122}\frac{\partial\chi_2^{12}}{\partial y_2}\right)\frac{\partial v_1}{\partial y_1}\\ &\quad + E_{1212}\left(\frac{\partial\chi_1^{12}}{\partial y_2} + \frac{\partial\chi_2^{12}}{\partial y_1}\right)\left(\frac{\partial v_1}{\partial y_2} + \frac{\partial v_2}{\partial y_1}\right)\\ &\quad + \left(E_{1122}\frac{\partial\chi_1^{12}}{\partial y_1} + E_{2222}\frac{\partial\chi_2^{12}}{\partial y_2}\right)\frac{\partial v_2}{\partial y_2}\Bigg]\mathrm{d}\,Y\\ &= \int_Y E_{1212}\left(\frac{\partial v_1}{\partial y_1} + \frac{\partial v_2}{\partial y_2}\right)\mathrm{d}\,Y,\end{aligned} \tag{30}$$

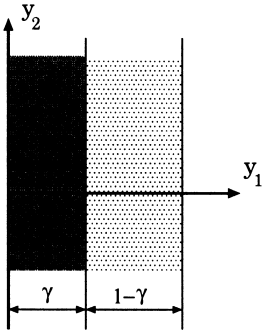

Fig. 5. A rank-1 layered material.

and from Eq. (23) for $i = 1$ and $j = 2$ it follows that:

$$E^{\mathrm{H}}_{1212} = \frac{1}{|Y|}\int_Y E_{1212}\left(1 - \frac{\partial \chi^{12}_1}{\partial y_2} - \frac{\partial \chi^{12}_2}{\partial y_1}\right)\mathrm{d}Y. \tag{31}$$

3.1. Rank-1 materials

Fig. 5 illustrates a rank-1 material comprising of layers in the y_2 direction and repeated periodically along the y_1 axis. In this case, the unit cell $\mathbf{Y} =]0,1[\times\mathbb{R}$ consists of two isotropic materials with relative thicnesses γ (strong material) and $1-\gamma$ (weak material). We note that the **Y**-periodicity assumption implies that χ^{kl} and the test functions v^i are independent of the y_2 coordinate.

case a:

Now considering case (a) and making use of the fact that the functions χ and v are only dependent on y_1, and using test functions $\mathbf{v} = [\pi(y_1),0^{\mathrm{T}}$, from Eq. (24) it follows that:

$$\int_Y E_{1111}\frac{\partial \chi^{11}_1}{\partial y_1}\frac{\partial v_1}{\partial y_1}\mathrm{d}Y = \int_Y E_{1111}\frac{\partial v_1}{\partial y_1}\mathrm{d}Y, \tag{32}$$

or

$$\int_Y \left(E_{1111}\frac{\partial \chi^{11}_1}{\partial y_1} - E_{1111}\right)\frac{\partial v_1}{\partial y_1}\mathrm{d}Y = 0. \tag{33}$$

According to the fact that the integral of the derivative of a periodic function over the period is zero (see Fact (2) in Section of Ref. [25]), as v_1 is **Y**-periodic:

$$\int_Y \frac{\partial v_1}{\partial y_1}\mathrm{d}Y = 0. \tag{34}$$

A comparison of Eqs. (33) and (34) results in:

$$E_{1111}\frac{\partial \chi^{11}_1}{\partial y_1} - E_{1111} = C_1, \tag{35}$$

where C_1 is a constant. Rearranging Eq. (35) as

$$\frac{\partial \chi^{11}_1}{\partial y_1} = 1 + \frac{C_1}{E_{1111}}, \tag{36}$$

from **Y**-periodicity of χ^{11} (also Fact 2 in Section 3 of Ref. [25]) we obtain:

$$C_1 = -\frac{1}{\dfrac{1}{|Y|}\displaystyle\int_Y \frac{\mathrm{d}y}{E_{1111}}}. \tag{37}$$

If we use the following notation for the volumetric average of a function f over Y,

$$\langle f\rangle = \frac{1}{|Y|}\int_Y f(y)\mathrm{d}y, \tag{38}$$

then Eq. (37) can be written as:

$$C_1 = -\left\langle\frac{1}{E_{1111}}\right\rangle^{-1} \tag{39}$$

Also, Eq. (25) yields

$$E^{\mathrm{H}}_{1111} = \frac{1}{|Y|}\int_Y \left(E_{1111} - E_{1111}\frac{\partial \chi^{11}_1}{\partial y_1}\right)\mathrm{d}Y = -C_1, \tag{40}$$

and consequently,

$$E^{\mathrm{H}}_{1111} = \left\langle\frac{1}{E_{1111}}\right\rangle^{-1}, \tag{41}$$

or by the compact notation

$$\boxed{D^{\mathrm{H}}_{11} = \langle D^{-1}_{11}\rangle^{-1}}. \tag{42}$$

case b:

Similarly, in case (b), by assuming the same test functions as before, from Eq. (27) we obtain:

$$\int_Y \left(E_{1111}\frac{\partial \chi^{22}_1}{\partial y_1} - E_{1122}\right)\frac{\partial v_1}{\partial y_1}\mathrm{d}Y = 0, \tag{43}$$

which gives

$$E_{1111}\frac{\partial \chi^{22}_1}{\partial y_1} - E_{1122} = C_2, \tag{44}$$

or

$$\frac{\partial \chi^{22}_1}{\partial y_1} = \frac{E_{1122}}{E_{1111}} + \frac{C_2}{E_{1111}}. \tag{45}$$

Integrating this equation on Y (and using Fact (2) in Section 3 of Ref. [25]) results in:

$$\frac{1}{|Y|}\int_Y \left(\frac{E_{1122}}{E_{1111}} + \frac{C_2}{E_{1111}}\right)\mathrm{d}Y = 0, \tag{46}$$

or

$$C_2\left\langle\frac{1}{E_{1111}}\right\rangle+\left\langle\frac{E_{1122}}{E_{1111}}\right\rangle=0, \tag{47}$$

$$C_2=-\left\langle\frac{E_{1122}}{E_{1111}}\right\rangle\left\langle\frac{1}{E_{1111}}\right\rangle^{-1}. \tag{48}$$

On the other hand, Eq. (28) yields

$$E^{\mathrm{H}}_{1122}=\frac{1}{|Y|}\int_Y\left(E_{1122}-E_{1111}\frac{\partial\chi_1^{22}}{\partial y_1}\right)\mathrm{d}Y. \tag{49}$$

Comparing Eqs. (49) and (44) one obtains

$$E^{\mathrm{H}}_{1122}=-C_2, \tag{50}$$

where using the compact notation we conclude that

$$\boxed{D^{\mathrm{H}}_{12}=\langle D_{12}D_{11}^{-1}\rangle\langle D_{11}^{-1}\rangle^{-1}}. \tag{51}$$

Now, since we know D^{H}_{11} and D^{H}_{12} from Eq. (29), it can be shown that

$$E^{\mathrm{H}}_{2222}=\frac{1}{|Y|}\int_Y\left(E_{2222}-E_{2211}\frac{\partial\chi_1^{22}}{\partial y_1}\right)\mathrm{d}Y, \tag{52}$$

and by introducing Eqs. (45) and (48) into Eq. (52), and using the compact notation we obtain

$$\boxed{D^{\mathrm{H}}_{22}=\langle D_{22}\rangle-\langle D_{12}^2D_{11}^{-1}\rangle+\langle D_{12}D_{11}^{-1}\rangle^2\langle D_{11}^{-1}\rangle^{-1}}. \tag{53}$$

case c:

Finally, considering case (c) where $k=1$ and $l=2$, and using $\mathbf{v}=[0,\ \pi(y_1)]^{\mathrm{T}}$ as the test function, Eq. (30) yields

$$\int_Y\left(E_{1212}\frac{\partial\chi_2^{12}}{\partial y_1}-E_{1212}\right)\frac{\partial v_2}{\partial y_1}\mathrm{d}Y=0, \tag{54}$$

which following the same procedure as before results in:

$$E_{1212}\frac{\partial\chi_2^{12}}{\partial y_1}-E_{1212}=C_3, \tag{55}$$

and as for the last two cases it is concluded that

$$C_3=-\left\langle\frac{1}{E_{1212}}\right\rangle^{-1}, \tag{56}$$

and from Eq. (31) it follows that

$$E^{\mathrm{H}}_{1212}=\frac{1}{|Y|}\int_Y E_{1212}\left(1-\frac{\partial\chi_2^{12}}{\partial y_1}\right)\mathrm{d}Y=-C_3. \tag{57}$$

Therefore, from Eqs. (56) and (57) and using the compact notation we obtain

$$\boxed{D^{\mathrm{H}}_{66}=\langle D_{66}^{-1}\rangle^{-1}}. \tag{58}$$

For the unit cell of Fig. 5, consisting of material I (strong) and material II (weak) with thicknesses γ and $1-\gamma$, respectively, from Eq. (42) it follows that

$$D^{\mathrm{H}}_{11}=\langle D_{11}^{-1}\rangle^{-1}=1\Big/\left[\int_0^{\gamma}\frac{\mathrm{d}y_1}{D^{\mathrm{II}}_{11}}+\int_{\gamma}^{1}\frac{\mathrm{d}y_1}{D^{\mathrm{II}}_{11}}\right], \tag{59}$$

$$D^{\mathrm{H}}_{11}=\frac{D^{\mathrm{I}}_{11}D^{\mathrm{II}}_{11}}{\gamma D^{\mathrm{II}}_{11}+(1-\gamma)D^{\mathrm{I}}_{11}}. \tag{60}$$

Now let us define the following terms:

Arithmetic average $\bar{A}$. For all $\xi\in[0,\ 1]$, the arithmetic average of two real numbers r_1 and r_2 is defined as:

$$\bar{A}(r_1,r_2,\xi)=\xi r_1(1-\xi)r_2. \tag{61}$$

Harmonic average $\underline{A}$. For all $\xi\in[0,\ 1]$, the harmonic average of two real numbers r_1 and r_2 is defined as:

$$\underline{A}(r_1,r_2,\xi)=\frac{r_1r_2}{\xi r_2+(1-\xi)r_1}. \tag{62}$$

For positive values of r_1 and r_2, $\underline{A}\le\bar{A}$ and $\underline{A}=\bar{A}$ if and only if $r_1=r_2$. So by making use of the above definitions, Eq. (60) can be written as:

$$D^{\mathrm{H}}_{11}=\underline{A}(D^{\mathrm{I}}_{11},D^{\mathrm{II}}_{11},\gamma). \tag{63}$$

Similarly, from Eqs. (51), (53) and (58), respectively, it follows that

$$D^{\mathrm{H}}_{12}=\bar{A}(D^{\mathrm{I}}_{12}D^{\mathrm{I}-1}_{11},D^{\mathrm{II}}_{12}D^{\mathrm{II}-1}_{11},\gamma)\underline{A}(D^{\mathrm{I}}_{11},D^{\mathrm{II}}_{11},\gamma), \tag{64}$$

$$\begin{aligned}D^{\mathrm{H}}_{22}=&\bar{A}(D^{\mathrm{I}}_{22},D^{\mathrm{II}}_{22},\gamma)-\bar{A}(D^{\mathrm{I}^2}_{12}D^{\mathrm{I}-1}_{11},D^{\mathrm{II}2}_{12}D^{\mathrm{II}-1}_{11},\gamma)\\&+\bar{A}^2(D^{\mathrm{I}}_{12}D^{\mathrm{I}-1}_{11},D^{\mathrm{II}}_{12}D^{\mathrm{II}-1}_{11},\gamma)\underline{A}(D^{\mathrm{I}}_{11},D^{\mathrm{II}}_{11},\gamma),\end{aligned}$$

and

$$D^{\mathrm{H}}_{66}=\underline{A}(D^{\mathrm{I}}_{66},D^{\mathrm{II}}_{66},\gamma). \tag{66}$$

If the materials are isotropic with the same Poisson's ratio and different Young's moduli E^{I} and E^{II}, then

$$D^i_{11}=D^i_{22}=\frac{E^i}{1-\nu^2};\quad D^i_{12}=\frac{\nu}{1-\nu^2}E^i;$$
$$D^i_{66}=\frac{E^i}{2(1+\nu)}\quad(i=\mathrm{I},\ \mathrm{II}).$$

In this case, by using Eqs. (63)–(66) one obtains

$$\mathbf{D}^{\mathrm{H}} = \begin{bmatrix} J_1 & vJ_1 & 0 \\ vJ_1 & J_2 + v^2 J_1 & 0 \\ 0 & 0 & (1-v)/2J \end{bmatrix}, \tag{67}$$

where

$$J_1 = \frac{1}{1-v^2}\underline{A}(E^{\mathrm{I}}, E^{\mathrm{II}}, \gamma); \quad J_2 = \bar{A}(E^{\mathrm{I}}, E^{\mathrm{II}}, \gamma).$$

In the particular case when the weak material is completely void (i.e. $E_{\mathrm{II}} = 0$), we have $J_1 = 0$ and $J_2 = \gamma E^{\mathrm{I}}$. Thus, Eq. (67) becomes:

$$\mathbf{D}^{\mathrm{H}} = \begin{bmatrix} 0 & 0 & 0 \\ 0 & \gamma E^{\mathrm{I}} & 0 \\ 0 & 0 & 0 \end{bmatrix}. \tag{68}$$

3.2. Rank-2 materials

As expalined in Section 2.2, the rank-1 material can be used as one of the components of a rank-2 material (see Fig. 3). Having relative thicknesses μ for the strong material and $1-\mu$ for the already-constructed rank-1 material, as shown in Fig. 6, by recursive use of Eqs. (63)–(66) the elements of the elasticity matrix can easily be found.

For example, assuming isotropy for the solid part of material with the Young's modulus E and Poisson's ratio v, and noticing that the directions of the rank0-1 layers and the solid layers are perpendicular, from Eq. (63) it follows that

$$D_{11}^{\mathrm{H}} = \underline{A}(D_{11}^{\mathrm{I}}, D_{22}^{\mathrm{R1}}, \mu), \tag{69}$$

where $D_{11}^{\mathrm{I}} = E/(1-v^2)$ and $D_{22}^{\mathrm{R1}} = \gamma E$. Here, R1 stands for the rank-1 material, also see seqn (68). Therefore, using Eq. (62) we obtain:

$$D_{11}^{\mathrm{H}} = \frac{\gamma E}{(1-\mu)+\gamma\mu(1-v^2)}. \tag{70}$$

Similarly, the other elements of the homogenized matrix can easily be found,

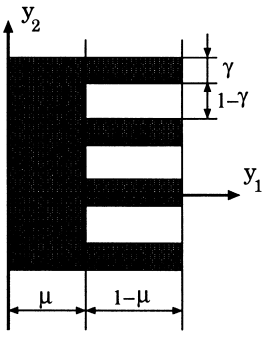

Fig. 6. Rank-2 material.

$$\mathbf{D}^{\mathrm{H}} = \frac{E}{(1-\mu)+\gamma\mu(1-v^2)} \begin{bmatrix} \gamma & \mu\gamma v & 0 \\ \mu\gamma v & \mu(1-\mu+\mu\gamma) & 0 \\ 0 & 0 & 0 \end{bmatrix}. \tag{71}$$

In practice, in order to avoid singularity in the optimization algorithm, the voids are replaced with a very weak material. The contribution of this material to the homogenized matrix can easily be calculated using the procedure described earlier.

3.3. Bi-material rank-2 composites

Referring to Fig. 4 and the instructions for the construction of the bi-material rank-2 composites; and using the superscripts I, II, V, III and R1 for the stiffer solid, the less stiff solid, the very weak material which represents the voids, the composite comprising two solids [Fig. 4(a)] and the rank-1 bi-material, respectively, b recursivel recalling Eqs. (63)–(66) and noticing that the axes of the rank-1 bi-material and the material I are perpendicular to each other, we obtain:

$$D_{11}^{\mathrm{H}} = \underline{A}(D_{11}^{\mathrm{I}}, D_{22}^{\mathrm{R1}}, \mu), \tag{72}$$

where

$$D_{22}^{\mathrm{R1}} = \bar{A}(D_{22}^{\mathrm{I\,II}}, D_{22}^{\mathrm{V}}, \gamma_2) - \bar{A}(D_{12}^{\mathrm{I\,II}^2} D_{11}^{\mathrm{I\,II}^{-1}}, D_{12}^{\mathrm{V}^2} D_{11}^{\mathrm{V}^{-1}}, \gamma_2) + \bar{A}^2(D_{12}^{\mathrm{I\,II}} D_{11}^{\mathrm{I\,II}^{-1}}, D_{12}^{\mathrm{V}} D_{11}^{\mathrm{V}^{-1}}, \gamma_2)\, \underline{A}(D_{11}^{\mathrm{I\,II}}, D_{11}^{\mathrm{V}}, \gamma_2) \tag{73}$$

and $D_{11}^{\mathrm{III}}, \ldots, D_{66}^{\mathrm{III}}$ are directly derived from Eqs. (63)–(66). For example,

$$D_{11}^{\mathrm{I\,II}} = \underline{A}(D_{11}^{\mathrm{I}}, \gamma_1) \quad \cdots$$

Similarly,

$$D_{12}^{\mathrm{H}} = \bar{A}(D_{12}^{\mathrm{I}} D_{11}^{\mathrm{I}^{-1}}, D_{12}^{\mathrm{R1}} D_{22}^{\mathrm{R1}^{-1}}, \mu)\underline{A}(D_{11}^{\mathrm{I}}, D_{22}^{\mathrm{II}}, \mu), \tag{74}$$

$$D_{22}^{\mathrm{H}} = \bar{A}(D_{22}^{\mathrm{I}}, D_{11}^{\mathrm{R1}}, \mu) - \bar{A}(D_{12}^{\mathrm{I}^2} D_{11}^{\mathrm{I}^{-1}}, D_{12}^{\mathrm{R1}^2} D_{22}^{\mathrm{R1}^{-1}}, \mu) + \bar{A}^2(D_{22}^{\mathrm{I}} D_{11}^{\mathrm{I}^{-1}}, D_{12}^{\mathrm{R1}} D_{22}^{\mathrm{R1}^{-1}}, \mu)\, \underline{A}(D_{11}^{\mathrm{I}}, D_{22}^{\mathrm{R1}}, \mu). \tag{75}$$

Finally,

$$\boxed{D_{66}^{\mathrm{H}} = \bar{A}(D_{66}^{\mathrm{I}}, D_{66}^{\mathrm{R1}}, \mu)}. \tag{76}$$

4. Numerical Solution Of The Homogenized Equation For A Cellular Body With Rectangular Holes

For most geometries of the base cell, the homogenization equations have to be solved by numerical techniques such as the finite element, boundary element or spectral method. In the next section, the derivation of the finite element formulation for 2D problems is explained.

4.1. Finite element formulation

Following a procedure similar to the analytical solution, the same three cases are considered.

case a: $k = 1$, $l = 1$

For the sake of simplicity, by using the compact notation and $\chi_1^{11} = \Phi_1$ and $\chi_2^{11} = \Phi_2$, Eqs. (24) and (25) will become:

$$\begin{aligned}
&\int_Y \Bigg[\left(D_{11}\frac{\partial \Phi_1}{\partial y_1} + D_{12}\frac{\partial \Phi_2}{\partial y_2} \right)\frac{\partial v_1}{\partial y_1} \\
&\quad + D_{66}\left(\frac{\partial \Phi_1}{\partial y_2} + \frac{\partial \Phi_2}{\partial y_1} \right)\left(\frac{\partial v_1}{\partial y_2} + \frac{\partial v_2}{\partial y_1} \right) \\
&\quad + \left(D_{12}\frac{\partial \Phi_1}{\partial y_1} + D_{22}\frac{\partial \Phi_1}{\partial y_1} + D_{22}\frac{\partial \Phi_2}{\partial y_2} \right)\frac{\partial v_2}{\partial y_2} \Bigg] \mathrm{d}Y \\
&= \int_Y \left(D_{11}\frac{\partial v_1}{\partial y_1} + D_{12}\frac{\partial v_2}{\partial y_2} \right) \mathrm{d}Y
\end{aligned} \tag{77}$$

and

$$D_{11}^{\mathrm{H}} = \frac{1}{|Y|}\int_Y \left(D_{11} - D_{11}\frac{\partial \Phi_1}{\partial y_1} - D_{12}\frac{\partial \Phi_2}{\partial y_2} \right) \mathrm{d}Y. \tag{78}$$

Rearranging Eq. (77) it follows that

$$\begin{aligned}
&\int_Y \begin{Bmatrix} \frac{\partial v_1}{\partial y_1} & \frac{\partial v_2}{\partial y_2} & \frac{\partial v_1}{\partial y_2} + \frac{\partial v_2}{\partial y_1} \end{Bmatrix} \begin{bmatrix} D_{11} & D_{12} & 0 \\ D_{12} & D_{22} & 0 \\ 0 & 0 & D_{66} \end{bmatrix} \\
&\quad \times \begin{Bmatrix} \partial \Phi_1/\partial y_1 \\ \partial \Phi_2/\partial y_2 \\ \partial \Phi_1/\partial y_2 + \partial \Phi_2/\partial y_1 \end{Bmatrix} \mathrm{d}Y \\
&= \int_Y \begin{Bmatrix} \frac{\partial v_1}{\partial y_1} & \frac{\partial v_2}{\partial y_2} & \frac{\partial v_1}{\partial y_2} + \frac{\partial v_2}{\partial y_1} \end{Bmatrix} \begin{Bmatrix} D_{11} \\ D_{12} \\ 0 \end{Bmatrix} \mathrm{d}Y.
\end{aligned} \tag{79}$$

Now, let us define

$$\boldsymbol{\epsilon}(\mathbf{v}) = \begin{Bmatrix} \partial v_1/\partial y_1 \\ \partial v_2/\partial y_2 \\ \partial v_1/\partial y_2 + \partial v_2/\partial y_1 \end{Bmatrix},$$

$$\boldsymbol{\epsilon}(\boldsymbol{\Phi}) = \begin{Bmatrix} \partial \Phi_1/\partial y_1 \\ \partial \Phi_2/\partial y_2 \\ \partial \Phi_/\partial y_2 + \partial \Phi_2/\partial y_1 \end{Bmatrix} \tag{80}$$

and

$$\mathbf{D} = [\mathbf{d}_1 \quad \mathbf{d}_2 \quad \mathbf{d}_3], \tag{81}$$

where $\mathbf{d}_1$, $\mathbf{d}_2$ and $\mathbf{d}_3$ are the columns of the elasticity matrix $\mathbf{D}$, so that

$$\mathbf{d}_1 = \begin{Bmatrix} D_{11} \\ D_{12} \\ 0 \end{Bmatrix}, \quad \mathbf{d}_2 = \begin{Bmatrix} D_{12} \\ D_{22} \\ 0 \end{Bmatrix} \quad \text{and} \quad \mathbf{d}_3 = \begin{Bmatrix} 0 \\ 0 \\ D_{66} \end{Bmatrix}. \tag{82}$$

Using the above definitions, Eq. (79) can be written as:

$$\int_Y \boldsymbol{\epsilon}^{\mathrm{T}}(\mathbf{v})\, \mathbf{D}\, \boldsymbol{\epsilon}(\boldsymbol{\Phi})\, \mathrm{d}Y = \int_Y \boldsymbol{\epsilon}^{\mathrm{T}}(\mathbf{v})\, \mathbf{d}_1\, \mathrm{d}Y, \quad \forall \mathbf{v} \in \mathbf{V}_{\mathrm{Y}} \tag{83}$$

and similarly Eq. (78) becomes:

$$\boxed{D_{11}^{\mathrm{H}} = \frac{1}{|Y|}\int_Y (D_{11} - \mathbf{d}_1^{\mathrm{T}}\boldsymbol{\epsilon}(\Phi))\, \mathrm{d}Y}. \tag{84}$$

Now we can apply the usual finite element method [26–29]. Discretizing the domain of the base cell and using global shape functions we can write:

$$\mathbf{v} = \sum_{i=1}^{N} \mathbf{N}_i^{\mathrm{g}} \hat{\mathbf{v}}_i = \mathbf{N}^{\mathrm{g}} \hat{\mathbf{v}}, \tag{85}$$

$$\boldsymbol{\Phi} = \sum_{i-1}^{N} \mathbf{N}_i^{\mathrm{g}} \hat{\boldsymbol{\Phi}}_i = \mathbf{N}^{\mathrm{g}} \hat{\boldsymbol{\Phi}}, \tag{86}$$

where

$$\mathbf{v} = [v_1, v_2]^{\mathrm{T}}, \qquad \boldsymbol{\Phi} = [\Phi_1, \Phi_2]^{\mathrm{T}} \tag{87}$$

$$\hat{\mathbf{v}}_i = [v_{1,i}, v_{2i}]^{\mathrm{T}}, \qquad \boldsymbol{\Phi} = [\Phi_{1i}, \Phi_{2i}]^{\mathrm{T}} \tag{88}$$

$$\hat{\mathbf{v}} = [\hat{\mathbf{v}}_1, \hat{\mathbf{v}}_2, \cdots, \hat{\mathbf{v}}_N]^{\mathrm{T}}, \quad \hat{\boldsymbol{\Phi}} = [\hat{\boldsymbol{\Phi}}_1, \hat{\boldsymbol{\Phi}}_1, \cdots, \hat{\boldsymbol{\Phi}}_1]^{\mathrm{T}} \tag{89}$$

and

$$\mathbf{N}_i^{\mathrm{g}} = \begin{bmatrix} 1 & 0 \\ 0 & 1 \end{bmatrix} N_i^{\mathrm{g}}, \tag{90}$$

where N_i^{g} is the global shape function associated with node i and N is the number of nodes in the whole discretized domain. Applying this approximation to Eq. (80) results in:

$$\boldsymbol{\epsilon}(\mathbf{v}) = \mathbf{L}\mathbf{v} = \mathbf{L}\mathbf{N}^{\mathrm{g}}\hat{\mathbf{v}} = \mathbf{L}\hat{\mathbf{v}}, \tag{91}$$

$$\boldsymbol{\epsilon}(\boldsymbol{\Phi}) = \mathbf{L}\boldsymbol{\Phi} = \mathbf{L}\mathbf{N}^{\mathrm{g}}\hat{\boldsymbol{\Phi}} = \mathbf{B}\hat{\boldsymbol{\Phi}}, \tag{92}$$

where $\mathbf{L}$ is the matrix of linear differential operators defined as:

$$\mathbf{L} = \begin{bmatrix} \partial/\partial y_1 & 0 \\ 0 & \partial/\partial y_2 \\ \partial/\partial y_2 & \partial/\partial y_1 \end{bmatrix}, \tag{93}$$

and

$$\mathbf{B} = \mathbf{L}\mathbf{N}^{\mathrm{g}} \tag{94}$$

is the global strain matrix.

Now, substituting Eqs. (93) and (94) into Eq. (83), we obtain:

$$\hat{\mathbf{v}}^{\mathrm{T}} \int_Y \mathbf{B}^{\mathrm{T}}\mathbf{D}\mathbf{B}\,\mathrm{d}Y\,\hat{\boldsymbol{\Phi}} = \hat{\mathbf{v}}^{\mathrm{T}} \int_Y \mathbf{B}^{\mathrm{T}}\mathbf{d}_1 \mathrm{d}Y, \quad \forall \mathbf{v}. \tag{95}$$

As $\mathbf{v}$ is an arbitrary test function, by removing $\hat{\mathbf{v}}$ from both sides of Eq. (95) we obtain:

$$\int_Y \mathbf{B}^{\mathrm{T}}\mathbf{D}\mathbf{B}\,\mathrm{d}Y\,\hat{\boldsymbol{\Phi}} = \int_Y \mathbf{B}^{\mathrm{T}}\mathbf{d}_1\,\mathrm{d}Y, \tag{96}$$

which is very similar to the well-known stiffness equation

$$\boxed{\mathbf{K}\hat{\boldsymbol{\Phi}} = \mathbf{f}}, \tag{97}$$

where the stiffness matrix is written as

$$\mathbf{K} = \int_Y \mathbf{B}\mathbf{D}\mathbf{B}\,\mathrm{d}Y \tag{98}$$

and the "force" vector has the form

$$\mathbf{f} = \int_Y \mathbf{B}^{\mathrm{T}}\mathbf{d}_1\,\mathrm{d}Y. \tag{99}$$

If n-node elements are used to discretize the domain, then within a typical element e:

$$\boldsymbol{\Phi} = \sum_{i=1}^{n} \mathbf{N}_i^e \hat{\boldsymbol{\Phi}}_i, \tag{100}$$

where

$$\mathbf{N}_i^e = \begin{bmatrix} 1 & 0 \\ 0 & 1 \end{bmatrix} N_i^e \quad \text{and} \quad \hat{\boldsymbol{\Phi}}_i = \begin{Bmatrix} \hat{\Phi}_{1i} \\ \hat{\Phi}_{2i} \end{Bmatrix}, \tag{101}$$

and where N_i^e is the shape function asociated with node i of the element e, and n is the number of nodes of each element. From Eq. (100) it follows that

$$\boldsymbol{\epsilon}(\boldsymbol{\Phi}) = \sum_{i=1}^{n} \mathbf{B}_i^e \hat{\boldsymbol{\Phi}}_i, \tag{102}$$

where

$$\mathbf{B}_i^e = \begin{bmatrix} \partial N_i^e/\partial y_1 & 0 \\ 0 & \partial N_i^e/\partial y_2 \\ \partial N_i^e/\partial y_2 & \partial N_i^e/\partial y_1 \end{bmatrix}. \tag{103}$$

Eq. (103) enables us to find the submatrix of the stiffness matrix of element e linking nodes i and j:

$$\boxed{\mathbf{k}_{ij}^e = \int_{Y^e} \mathbf{B}_i^e \mathbf{D} \mathbf{B}_j^e \mathrm{d}Y}, \tag{104}$$

where Y^e denotes the volume of element. Also the nodal forces of element e associated with node i are obtained from:

$$\boxed{\mathbf{f}_i^e = \int_{Y^e} \mathbf{B}_i^{e\mathrm{T}} \mathbf{d}_1\,\mathrm{d}Y}. \tag{105}$$

We also note that the global stiffness matrix and the global forces can be assembled from the element stiffnes matrices and force vectors:

$$\mathbf{K} = \mathop{\mathbf{A}}_{e=1}^{m} \mathbf{k}^e, \tag{106}$$

$$\mathbf{f} = \mathop{\mathbf{A}}_{e=1}^{m} \mathbf{f}^e, \tag{107}$$

where $\mathbf{A}_{e=1}^{m}$ stands for the finite element assembly operator and m is the number of elements.

It is interesting to notice that the "force" vector used in homogenization has a physical meaning and it is, in fact, a specific case of *initial strain loading*. To demonstrate this we recall that the nodal forces induced by initial strains are (Refs [27, 29]):

$$\{f_i^{\epsilon^0}\}^e = \int_{Y^e} \mathbf{B}^{e\mathrm{T}} \mathbf{D} \boldsymbol{\epsilon}^0\,\mathrm{d}Y. \tag{108}$$

Now, comparing Eqs. (108) and (105) results in

$$\mathbf{D}\boldsymbol{\epsilon}^0 = \mathbf{d}_1, \tag{109}$$

or

$$\begin{bmatrix} D_{11} & D_{12} & 0 \\ D_{12} & D_{22} & 0 \\ 0 & 0 & D_{66} \end{bmatrix} \begin{Bmatrix} \epsilon^0_{11} \\ \epsilon^0_{22} \\ 2\epsilon^0_{12} \end{Bmatrix} = \begin{Bmatrix} D_{11} \\ D_{12} \\ 0 \end{Bmatrix}, \tag{110}$$

which implies that

$$\boxed{\epsilon^0_{11} = 1, \quad \epsilon^0_{22} = 0 \quad \text{and} \quad \epsilon^0_{12} = 0}. \tag{111}$$

Thus, in this case, the loading is a unit initial strain in only the y_1 direction.

If Eq. (98) is solved to give the displacements $\hat{\mathbf{\Phi}}$ and strains $\boldsymbol{\epsilon}(\hat{\mathbf{\Phi}})$, then using Eq. (84) the first element of the homogenized matrix D^{H}_{11} can be calculated.

case b: $k = 2$, $l = 2$

Starting from Eq. (27) and following the same procedure as for case (a), and representing χ^{22}_1 as Ψ_1 and χ^{22}_2 as Ψ_2, one obtains:

$$\int_Y \boldsymbol{\epsilon}^{\mathrm{T}}(\mathbf{v})\, \mathbf{D}\, \boldsymbol{\epsilon}(\mathbf{\Psi})\, \mathrm{d}Y = \int_Y \boldsymbol{\epsilon}^{\mathrm{T}}(\mathbf{v}) \mathbf{d}_2\, \mathrm{d}Y, \quad \forall \mathbf{v}. \tag{112}$$

Then, using the same steps as for case (a), we obtain

$$\boxed{\mathbf{K}\hat{\mathbf{\Psi}} = \mathbf{f}}. \tag{113}$$

In this case, the formulae for the stiffness matrix are the same a for case (a) and the only difference is in loading. The nodal forces become

$$\boxed{\mathbf{f}^e_i = \int_{Y^e} \mathbf{B}^{e\mathrm{T}}_i \mathbf{d}_2\, \mathrm{d}Y}, \tag{114}$$

which implies a unit initial strain in the y_2 direction, so that

$$\boxed{\epsilon^0_{11} = 0, \quad \epsilon^0_{22} = 1 \quad \text{and} \quad \epsilon^0_{12} = 0}. \tag{115}$$

On the other hand, following a similar process, Eqs. (28) and (29) can be written as:

$$\boxed{D^{\mathrm{H}}_{12} = \frac{1}{|Y|}\int_Y [D_{12} - \mathbf{d}^{\mathrm{T}}_1 \boldsymbol{\epsilon}(\mathbf{\Psi})]\, \mathrm{d}Y}, \tag{116}$$

$$\boxed{D^{\mathrm{H}}_{22} = \frac{1}{|Y|}\int_Y [D_{22} - \mathbf{d}^{\mathrm{T}}_2 \boldsymbol{\epsilon}(\mathbf{\Psi})]\, \mathrm{d}Y}. \tag{117}$$

Having obtained the displacement function $\hat{\mathbf{\Psi}}$ and the strain $\boldsymbol{\epsilon}(\hat{\mathbf{\Psi}})$ by solving Eq. (113), from Eqs. (116) and (117) D^{H}_{12} and D^{H}_{22} can be obtained.

case c: $k = 1$, $l = 2$

As for cases (a) and (b) we use the compact notation and rename χ^{12}_1 and χ^{12}_2 respectively, as θ_1 and θ_2. From Eq. (30) it follows that

$$\int_Y \epsilon^{\mathrm{T}}(\mathbf{v})\, \mathbf{D}\, \boldsymbol{\epsilon}(\boldsymbol{\theta})\, \mathrm{d}Y = \int_Y \boldsymbol{\epsilon}^{\mathrm{T}}(\mathbf{v}) \mathbf{d}_3 \mathrm{d}Y, \quad \forall \mathbf{v}. \tag{118}$$

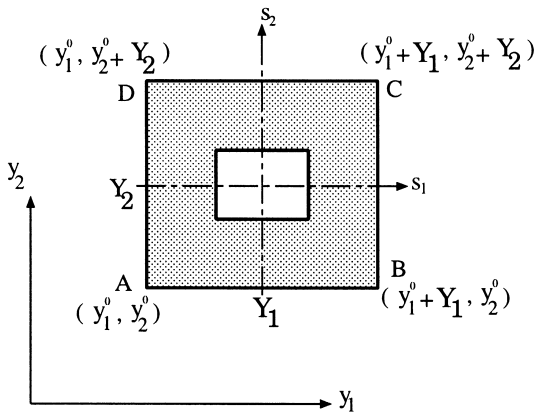

Fig. 7. The base cell of periodicity.

The nodal forces of elements in this case are

$$\boxed{\mathbf{f}^e_i = \int_{Y^e} B^e_i \mathbf{d}_3 \mathrm{d}Y}, \tag{119}$$

which implies a unit initial shear strain loading

$$\boxed{\epsilon^0_{11} = 0, \quad \epsilon^0_{22} = 0 \quad \text{and} \quad 2\epsilon^0_{12} = 1}. \tag{120}$$

Also, applying the above notation, Eq. (31) yields

$$\boxed{D^{\mathrm{H}}_{66} = \frac{1}{|Y|}\int_Y [D_{66} - \mathbf{d}^{\mathrm{T}}_3 \boldsymbol{\epsilon}(\boldsymbol{\theta})]\, \mathrm{d}Y}. \tag{121}$$

Thus, we have seen how the finite element formulation for calculation of the elements of the homogenized elasticity matrix is derived. Furthermore, we have observed that for 2D problems, by considering three

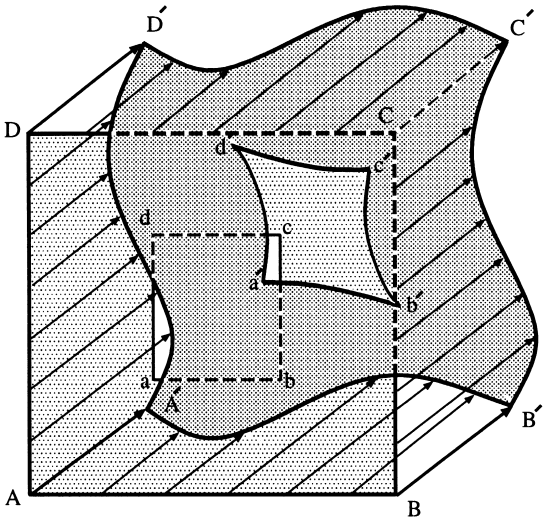

Fig. 8. A typical deformation of the base cell.

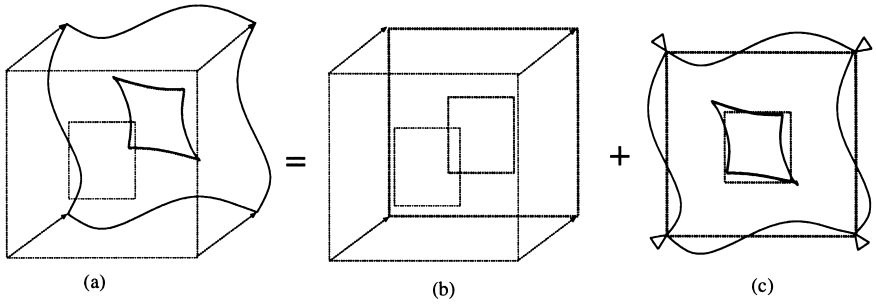

Fig. 9. Components of a possible microscopic displacement field.

loading cases it is possible to find all of the elasticity coefficients. In practice, after discretizing the domain of the base cell, it is sufficient to run the finite element program for different unit initial strain cases. Derivation of the required boundary conditions will be discussed in the following section.

4.2. Derivation of the boundary conditions from periodicity

So far we have concluded that the integral equation of homogenization, Eq. (22), is a boundary value problem and it can be reduced, after appropriate discretization, to the conventional form

$$\mathbf{K}\boldsymbol{\chi} = \mathbf{f}, \tag{122}$$

which has to be solved on the domain of the unit cell. Any boundary value problem to be solved needs some information about the initial or boundary conditons. To determine the appropriate boundary conditions, we reconsider the main assumption of homogenization theory, i.e. periodicity. The microscopic displacement field $\mathbf{x}$ is the $\mathbf{Y}$-periodic solution of Eq. (122). The base cell $\mathbf{Y}$ is illustrated in Fig. 7.

From the definition of periodicity [25], it follows that

$$\begin{aligned}\boldsymbol{\chi}(y_1, y_2) &= \boldsymbol{\chi}(y_1 + Y_1, y_2) = \boldsymbol{\chi}(y_1 + Y_1, y_2 + Y_2)\\ &= \boldsymbol{\chi}(y_1, y_2 + Y_2).\end{aligned} \tag{123}$$

Considering $y_1 = y_1^0$ and $y_2 = y_2^0$, we can write that

$$\begin{aligned}\boldsymbol{\chi}(y_1^0, y_2^0) &= \boldsymbol{\chi}(y_1^0 + Y_1, y_2^0) = \boldsymbol{\chi}(y_1^0 + Y_1, y_2^0 + Y_2)\\ &= \boldsymbol{\chi}(y_1^0, y_2^0 + Y_2),\end{aligned} \tag{124}$$

which states that the microscopic displacements of the corner points of the base cell are equal ($\overrightarrow{AA'} = \overrightarrow{BB'} = \overrightarrow{CC'} = \overrightarrow{DD'}$). A typical possible deformation of the base cell is exaggerated in Fig. 8. We notice that this displacement field can be resolved into two parts. One translation or rigid body motion [see Fig. 9(b)], which has no effect on the stress and strain fields inside the domain of the cell, and on in situ deformation [Fig. 9(c)]. In Fig. 10 a typical microscopic deformation for a group of $\mathbf{Y}$-periodic cells is schematically depicted.

If the components of $\boldsymbol{\chi}$ in the y_1 and y_2 directions, respectively, are denoted by the scalar displacement functions u and v, Eq. (123) can be written as:

$$\begin{aligned}u(y_1, y_2) &= u(y_1 + Y_1, y_2) = u(y_1 + Y_1, y_2)\\ &= u(y_1, y_2 + Y_2)\end{aligned} \tag{125}$$

$$\begin{aligned}v(y_1, y_2) &= v(y_1 + Y_1, y_2) = v(y_1 + Y_1, y_2 + Y_2)\\ &= v(y_1, y_2 + Y_2).\end{aligned} \tag{126}$$

So far, our discussion has been general and Eq. (124) is valid for any periodic cell of composite material. To obtain the proper boundary restrictions one can utilize the methods applied to the repeatable structures [30]. For example, the numbers of pairs of nodes located on the opposite edges of the cell can be linked so that opposite edges have identical deformed shapes. Alternatively, the Lagrange multiplier method [31] or the penalty method [31, 32] can be adopted. Here a direct method is presented [33, 34].

Here, we focus on cells with rectangular voids, which is the material model chosen for the topology optimization.[1] We remember that for 2D problems the

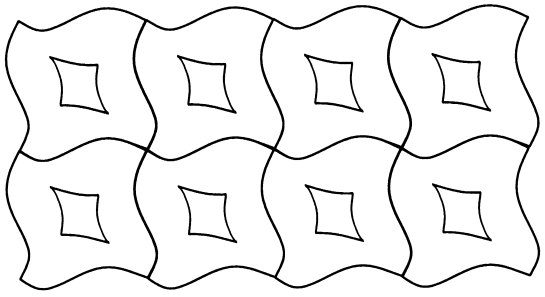

Fig. 10. A typical deformation of the cellular body.

[1] However, the following conclusions are valid for all periodic cells of composites which have two orthogonal axes of symmetry.

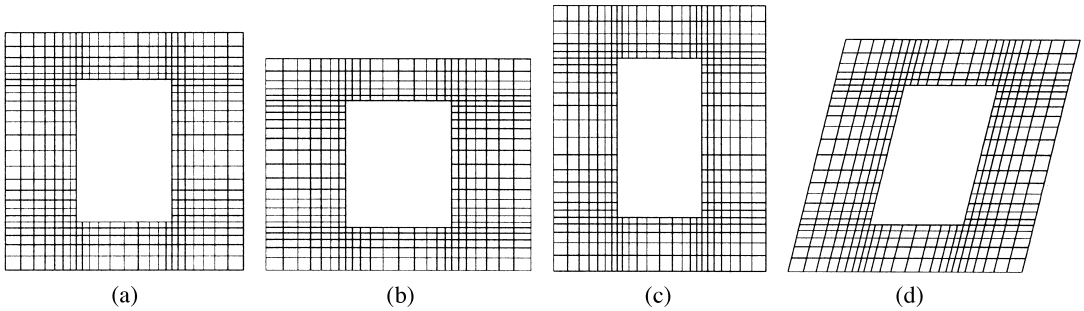

Fig. 11. (a) Base cell. (b) Deformation induced by unit initial strain in horizontal direction. (c) Deformation induced by unit initial strain in vertical direction. (d) Deformation induced by unit initial shear strain.

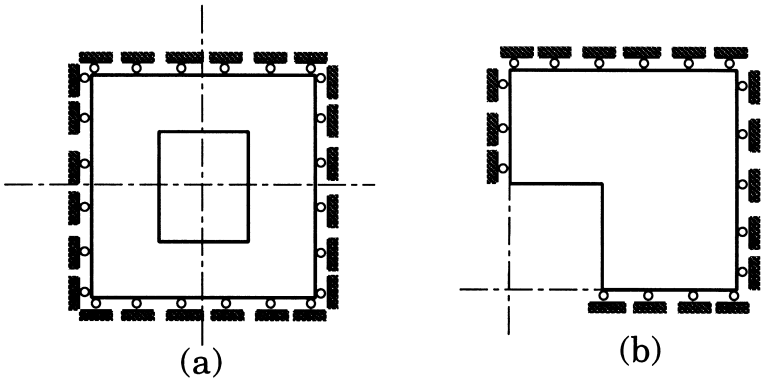

Fig. 12. Boundary conditions for cases (a) and (b).

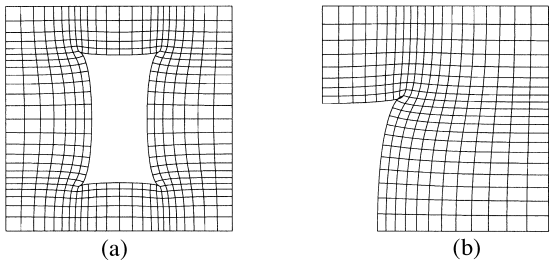

Fig. 13. (a) Deformation of the full cell. (b) Deformation of a quarter of the base cell.

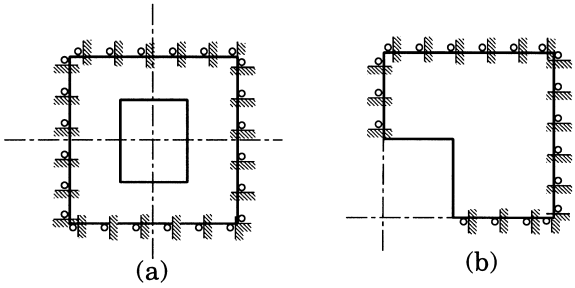

Fig. 15. Boundary conditions for case (c).

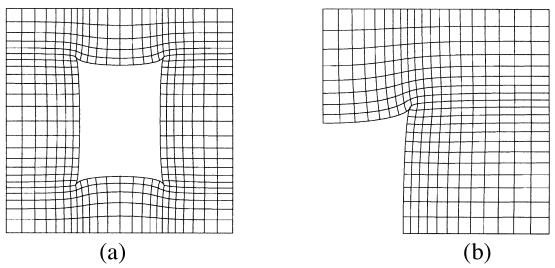

Fig. 14. (a) Deformation of the full cell. (b) Deformation of a quarter of the base cell.

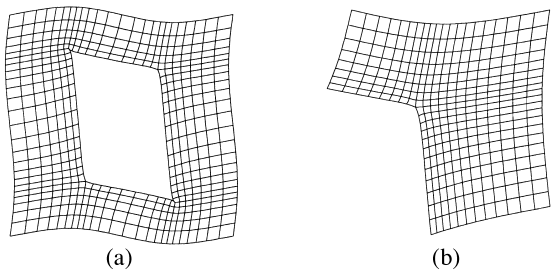

Fig. 16. (a) Deformation of the full cell. (b) Deformation of a quarter of the base cell.

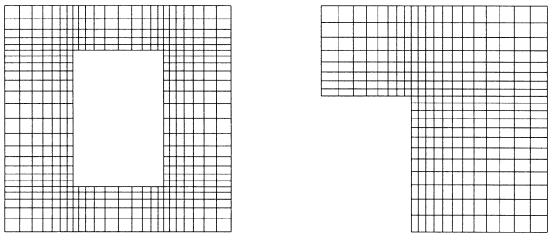

Fig. 17. (a) FE mesh for full cell. (b) FE mesh for a quarter of the base cell.

homogenization equation must be solved three times. The earlier cases are again considered here.

case a:

In unit cells with rectangular voids the geometry of the cell is symmetric with respect to the axes of symmetry s_1 and s_2, as illustrated in Fig. 7. Recalling Eq. (117), the loding to be imposed in this case is a uni initiao strain in the y_1 direction (i.e. $\epsilon^0_{11} = 1$, ϵ^0_{22} and $\epsilon^0_{12} = 0$). In Fig. 11(b) the deformation of the base cell under this loading is depicted. To prevent rigid body motion, the horizontal and vertical displacements of the bottom left corner, and the vertical displacement of the bottom right corner are restricted. For the displacements and the applied loading under consideration, we see that the symmetric condition is realized.

From the symmetry of geometry and loading with respect to s_2 (see Fig. 7), it follows that

$$u(y^0_1, y_2) = -u(y^0_1 + Y_1, y_2), \tag{127}$$

$$v(y^0_1, y_2) = v(y^0_1 + Y_1, y_2), \tag{128}$$

and similarly, from symmetry with respect to s_1 it follows that

$$u(y_1, y^0_2) = u(y_1, y^0_2 + Y_2), \tag{129}$$

$$v(y_1, y^0_2) = -v(y_1, y^0_2 + Y_2). \tag{130}$$

Comparing Eqs. (127) and (130) with Eqs. (125) and (126) results in

$$u(y^0_1, y_2) = u(y^0_1 + Y_1, y_2) = 0, \tag{131}$$

and

$$v(y_1, y^0_2) = v(y_1, y^0_2 + Y_2) = 0. \tag{132}$$

According to Eqs. (131) and (132) the horizontal displacement of the left- and right-hand side edges of the cell is restricted. Similarly, in the bottom and top edges of the cell the vertical displacement is zero. These boundary conditions are depicted in Fig. 12(a). We note that by utilizing symmetry only a quarter of the domain of the unit cell needs to be analysed; see Fig. 12(b).

We also note that in this case, from Eqs. (131) and (125), by substituting $y_1 = y^0_1$ and $y_2 = y^0_2$ it follows that:

$$\begin{aligned} u(y^0_1, y^0_2) &= u(y^0_1 + Y_1, y^0_2) = u(y^0_1 + Y_1, y^0_2 + Y_2) \\ &= u(y^0_1, y^0_2 + Y_2) = 0, \end{aligned} \tag{133}$$

and, similarly Eqs. (128) and (122) result in

$$\begin{aligned} v(y^0_1, y^0_2) &= v(y^0_1 + Y_1, y^0_2) = v(y^0_1 + Y_1, y^0_2 + Y_2) \\ &= v(y^0_1, y^0_2 + Y_2) = 0, \end{aligned} \tag{134}$$

which means that the rigid body motion does not happen. The deformation of the base cell is depicted in Fig. 13. As the deformations induced by unit initial strain are very large, they are scaled in the ratio 1:4.

case b:

As with case a), because of the symmetry of geometry and loading, we conclude the same boundary conditions. See Fig. 12. Deformation of the unconstrained cell is depicted in Fig. 11(c). In Fig. 14 the deformation of the full cell and a quarter cell are illustrated.

case c:

Recalling Eq. (120), the loading in this case is a unit initial shear strain ($\epsilon^0_{11} = 0$, $\epsilon^0_{22} = 0$ and $2\epsilon^0_{12} = 1$). The unconstrained deformation of the cell is shown in Fig. 11(d). In this case, the anti-symmetry condition

Table 1. Comparison of results

Mesh	D^H_{11}	D^H_{12}	D^H_{22}	D^H_{66}	Remarks
20 × 20 4-node	13.015	3.241	17.552	2.785	Ref. [35]
1st adapt	12.910	3.178	17.473	2.714	Ref. [35]
2nd adapt	12.865	3.146	17.437	2.683	Ref. [35]
3rd adapt.	12.844	3.131	17.421	2.668	Ref. [35]
436 8-node	12.839	3.139	17.422	2.648	HOMOG case (a)
305 8-node	12.820	3.124	17.407	2.634	HOMOG case (b)

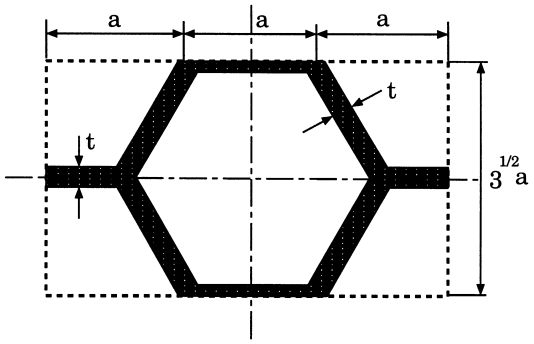

Fig. 18. Base cell of a composite with a honeycomb microstructure.

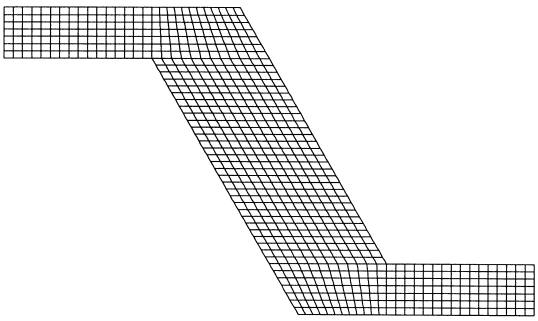

Fig. 19. FE mesh for a quarter of the honeycomb cell.

with respect to the axes of symmetry (s_1 and s_2 in Fig. 7) exists. This can be verified by noticing that the loading is uniform all over the domain of the cell, and for every element in one quadrant of the cell there are three similar ones in the other quadrants which exhibit the anti-symmetry condition.

From the anti-symmetry condition, the displacement of the opposite edges of the base cell may be expressed as:

$$u(y_1^0, y_2) = u(y_1^0 + Y_1, y_2), \tag{135}$$

$$v(y_1^0, y_2) = -v(y_1^0 + Y_1, y_2), \tag{136}$$

$$u(y_1, y_2^0) = -u(y_1, y_2^0 + Y_2), \tag{137}$$

$$v(y_1, y_2^0) = v(y_1, y_2^0 + Y_2). \tag{138}$$

Comparing Eqs. (135)–(138) with Eqs. (125) and (126) results in:

$$v(y_1^0, y_2) = v(y_1^0 + Y_1, y_2) = 0, \tag{139}$$

$$u(y_1, y_2^0) = u(y_1, y_2^0 + Y_2) = 0. \tag{140}$$

From Eq. (139) we observe that for the points located on the left- and right-hand side edges of the base cell, the vertical displacement is zero. According to Eq. (140) the nodes located on the bottom and top edges have zero horizontal displacement. These boundary conditions are illustrated in Fig. 15(a). Using the anti-symmetry conditions it is only necessary to consider a quarter of the cell with appropriate boundary conditions, as depicted in Fig. 15(b).

As with cases (a) and (b), by placing $y_1 = y_1^0$ and $y_2 = y_2^0$ in Eqs. (139), (140), (125) and (126) and comparing them, we again end up with Eqs. (133) and (134), which means that the outer corner points of the cell are fixed and the rigid body mode, as depicted in Fig. 9(b), does not appear. Deformation of the base cell and a quarter of it for this loading are illustrated in Fig. 16.

We note that because of similarities of the boundary conditions in cases (a)–(c), one can only define the boundary conditions for case (a), and for case (c), instead of defining a new problem, a few lines can be added to the finitre element (FE) code to change it automatically.

4.3. Examples

For the numerical solution of the homogenization equation by the finite element method a FORTRAN code (given the name HOMOG) was developed. Two examples are now presented.

Example 1: The first example, consists of a unit square base cell containing a 0.4×0.6 void (see Fig. 17) and with solid phase material properties $D_{11} = D_{22} = 30$ and $D_{12} = D_{66} = 10$ (all units are assumed to be consistent). This problem has been solved by Bendsøe and Kikuchi [35].

Table 2. Comparison of results

Mesh	D_{11}^{H}	D_{12}^{H}	D_{22}^{H}	D_{66}^{H}	Remarks
9072 4-node	0.0958	0.0713	0.0950	0.0125	Pixel-like discretization
9520 4-node	0.0968	0.0720	0.0968	0.0124	PREMAT2D
752 9-node	0.0966	0.0720	0.0966	0.0123	HOMOG

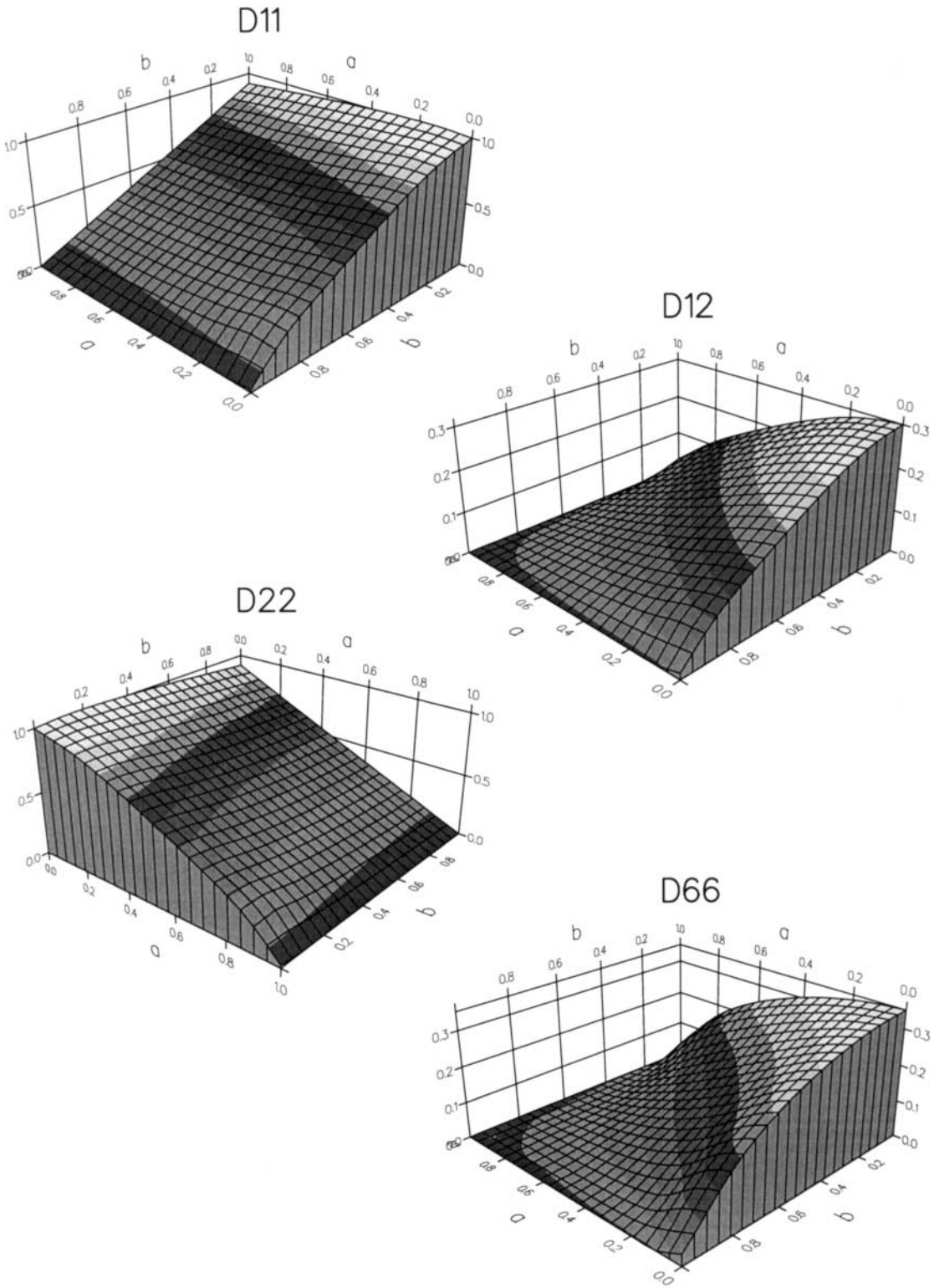

Fig. 20. Homogenized elasticity constants with respect to a and b.

This example was solved using two different meshes. First [case (a)] the mesh of Fig. 17(a) with 436 elements is used. In case (b), by making use of symmetry only a quarter of the cell was meshed with 305 elements, as shown in Fig. 17(b). When the problem was executed using one quarter of the mesh of Fig. 17(a), exactly the same results as case (a) were obtained. In all cases, 8-node elements were adopted. In Table 1 the results are compared with the solution of Bendsøe and Kikuhi. They used an initial 20×20 FE mesh and then applied the *h*-adaptation method three times.

Example 2: The problem of a cellular material with a perfect honeycomb base cell was solved by Sigmund [36]. The base cell is illustrated in Fig. 18. To ensure that the area of the base cell is unity, the dimension $a = 3^{-3/4}$ was chosen. In this example the ratio of the wall thickness to cell size is $t/a = \sqrt{3}/6$. The material is assumed to be isotropic with Young's modulus $E = 0.91$ and the Poisson's ratio $v = 0.3$. All units are assumed to be consistent.

Sigmund [36] has solved this problem considering a very weak material instead of a void, so that $E_{\text{void}}/E_{\text{solid}} = 10^{-4}$ His results using 9072 4-node elements are shown in the first row of Table 2. To compare his results, he also executed this example wih PREMAT2D developed by Guedes [37] with 9520 4-node elements.

In the last row of Table 2, the results obtained from running HOMOG are given. The mesh of Fig. 19 for only one quarter of the honeycomb cell with 752 9-node bi-quadratic elements was adopted.

4.4. Homogenized constitutive matrix for square microcells with rectangular voids

In order to carry out topology optimization using the model involving material with square microcells with rectangular holes, our aim is numerically solving the homogenization equations is to find how the constitutive matrix $\mathbf{D}^{\mathrm{H}}$ components vary in terms of the dimensions of the rectangular hole, i.e. to construct $\mathbf{D}^{\mathrm{H}}(a,b)$.

For this purpose a grid of 11×11 equally spaced sampling points for 121 values of a and b was contructed, and for each pair of values of a and b a finite element mesh was generated. The material is assumed to be isotropic with $E/(1-v) = 1$ scaled to equal unity and Poisson's ratio $v = 0.3$. The HOMOG code was executed for the generated finite element meshes. In all cases, the 8-node serendipity elements were adopted with 3×3 Gauss–Legendre integration. Variations of the elements of the elasticity matrix with respect to the dimensions of the holes are illustrated in Fig. 20.

4.5. Least square smoothing

To find the elements of the homogenized elasticity matrix in function form from the discrete values obtained at the sampling points, different interpolation techniques, such as splines, least squares approximation polynomials or shape functions can be used. Legendre polynomials were suggested by Bendsøe and Kikuchi [11, 35, 38]. In this work a conventional least squares data fitting method was employed.

If $D_p^n(a,b)$ is considered as the desirable approximating complete polynomial of degree n, it can be written as:

$$D_p^n(a,b) = \sum_{i=0}^{n}\sum_{j=0}^{n} c_k a^i b^j, \quad k = 1, 2, \cdots, \frac{n(n+1)}{2} = N, \tag{141}$$

where N is the number of terms of the approximating polynomial. The coefficients c_k can be found by minimizing

$$e(c_k) = \sum_{i=1}^{n_i}\sum_{j=1}^{n_1}[\hat{D}(a_i, b_j) - D_p^n(a,b)]^2, \tag{142}$$

where $\hat{D}(a_i,b_j)$ are the elements of the homogenized constitutive matrix at the sampling points and n_i and n_j are the number of points along the a and b axes of the sampling grid (in our case $n_i = n_j = 11$). Now from stationary conditions for Eq. (142), it follows that

$$\frac{\partial e(c_k)}{\partial c_k} = 0, \quad k = 1, 2, \cdots, N, \tag{143}$$

which provides a system of N linear equations from which the coefficients c_k can be calculated.

5. Conclusions And Final Remarks

In this second part of a three-paper review we have considered the motives for using the homogenization theory for topological structural optimization. Different material models have been described and the analytical solution of the homogenization equations for the so-called "rank laminate composites" have been presented. The finite element formulation has been explained for the material model, based on a microstructrue consisting of an isotropic material with rectangular voids. Some numerical examples have also been presented to illustrate the use of the method.

In the final part of this review, the mathematical model for the topological structural optimization will be constructed, and the derivation of the related optimality criteria will be explained. A modified resiz-

ing scheme will be suggested. Finally, some illustrative examples will be provided.

Acknowledgements

The moral and financial support of the Behim Dezh Co. and the University of Shahroud (Iran) is gratefully acknowledged.

References

[1] Cheng KT, Olhoff N. An investigation concerning optimal design of solid elastic plates. Int J Solids Struct 1982;16:305–23.
[2] Cheng KT, Olhoff N. Regularized formulation for optimal design of axisymetric plates. Int J Solids Struct 1982;18:13–70.
[3] Lurie KA, Chirkaev AV. G-clousure of some particular sets of admissible material characteristics for the problem of bending of thin plates. J Optim Theory Appl 1984;42:305–15.
[4] Rozvany CIN, Olhoff N, Bendsøe MP, Ong TG, Sandler R, Szto WT. Least-weight design of perforated elastic plates, parts i and ii. Int J Solids Struct 1987;23:521–50.
[5] Ong TG, Rozvany GIN, Szeto WT. Least-weight design of perforated elastic plates for given compliance: non-zero poisson's ratio. Comp Meth Appl Mech Engng 1988;66:301–22.
[6] Kohn RV, Strang G. Optimal design for torsional rigidity. In: Atluri SN, Gallaher RH, Zienkiewicz OC, editors. Hybrid and mixed finite element methods. New York: Wiley, 1982. p. 281–88.
[7] Rozvany GIN, Zhou M, Birker T. Generalized shape optimization without homogenization. Struct. Optim. 1992;4:250–52.
[8] Kohn RV, Strang G. Optimal design and relaxation of variational problems. Comm Pure Appl Math 1986; 39:113–37 (Part 1), 139–83 (Part II), 353–77 (Part III).
[9] Bendsøe MP. Optimal shape design as a material distribution problem. Struc Optim 1989;1:193–202.
[10] Bonnetier E, Vogelius M. Relaxation of a compliance functional for a plate optimization problem. Technical Report, University of Maryland, 1986.
[11] Bendøe MP, Díaz AR, Kikuchi N. Topology and generalized layout optimization of elastic structures. In: Bendsø MP, Mota Soares CA, editors. Topology design of structures. Dordrecht: Kluwer, 1993. p. 159–205.
[12] Avellaneda M. Optimal bounds and microgeometries for elastic two-phase composites. SIAM J Appl Math 1987;47:1216–28.
[13] Avellaneda M, Milton GW. Bounds on the effective elasticity tensor composites based on two-point correlation. In: Hui D, Kozik TJ, editors. Composite material technology. ASME, 1989. p. 89–93.
[14] Avellaneda M. Bounds on the effective elastic constants of two-plane composite materials. In: Brezis X, Lions JL, editors. Proceeings of the Seminar College at the College de France. London: Pitman, 1989.
[15] Allaire G, Kohn RV. Optimal bounds on the effective behavior of a mixture of two well ordered elastic materials. Q Appl Math 1993;51:643–674.
[16] Olhoff N, Kog L, Thomsen J. Bi-material topology optimization. In: Herskovites J, editor. Structural optimization 93. vol. 1. COPPE/Federal University of Rio de Janeiro, Rio de Janeiro, Brazil, 1993, p. 327–334.
[17] Thomsen J. Topology optimization of structures composed of one or two materials. Struct Optim 1992;5:108–15.
[18] Maute K, Ramm E. Adaptive techniques in topology optimization. In: Proceedings of Symposium on Multidisciplinary Analysis and Optimization. Panama City, Florida, USA, 1994.
[19] Rozvany GN, Bendsøe MP, Kirsh U. Layout optimization of structures. Appl Mech Rev 1995;48(2):41–119.
[20] Zhouu M, Rozvany CIN. The coc algorithm, part ii: topological, geometrical and generalized shape optimization. Comp Meth ppl Mech Engng 1991;89:309–35.
[21] Maute K, Ramm E. The genesis of continuum structures. In: Proceedings of the Third International Symposium of the SFB 230. Stuttgart, 1994.
[22] Maute K, Ramm E. Topology optimization of plate and shell structures. In: Proceedings of the IASS-ASCE International Symposium. Atlanta, Georgia, USA, 1994.
[23] Ramm E, Bletzinger KU, Reitinger R, Maute K. The challenge of structural optimization. In: Topping BHV, Papadrakakis M, editors. Advances in structural optimization, CIVIL-COMP. Edinburgh, 1994. p. 27–52.
[24] Rozvany GIN, editors. Shape and layout optimization of structural systems and optimality criteria methods. CISM, Udine: Springer, 1992.
[25] Hassani B, Hinton E. A review of homogenization and topology optmization—part i: Homogenization theory for media with periodic structure, Technical Report CR/883/95. Department of Ciil Engineering University of Wales Swansea, 1995.
[26] Hinton E, Owen DRJ. Intoduction to Finite Element Computations. Swansea: Pineridge Press, 1979.
[27] Zienkiewicz OC, Taylor RL. The finite element method, 4th ed. London: McGraw-Hill, 1989; vol. 1.
[28] Hughes TJR. The finite element method. Englewood Cliffs: Prentice-Hall, 1987.
[29] Hinton E, Owen DRJ. Finite element programming. London: Academic Press, 1977.
[30] Zienkiewicz OC, Scott FC. On the principle of repeatability and its application in alalysis of turbine and pump impellers. Int J Num Meth Engng 1972;4:445–52.
[31] Cook RD, Malkus DS, Plesha ME. Concepts and application of finite element analysis. 3rd ed. New York: Wiley, 1989.
[32] Sigmund O. Materials with prescribed constitutive parameters: an inverse homogenization problem, Technical Report 470. The Technical University of Denmark, 1993.
[33] Hassani B. Finite element solution of the homogenization equation for symmetric cells of periodicity, Technical Report CR/887/95. Department of Civil Engineering, 1995.

[34] Hassani B. A direct method to derive the boundary conditions of the homogenization equation for symmetric cells. Comm Numer Meth Engng 1996; 12: 185–196.
[35] Bendsøe MP, Kikuchi N. Generating optimal topologies in structural design using homogenization method. Comp Meth Appl Mech Engng 1988;71:197–224.
[36] Sigmund O. Design of material structures using topology optimization. PhD thesis. Technical University of Denmark, 1994.
[37] Guedes JM, Kikuchi N. Pre and post processing for materials based on the homogenization method with adaptive finite element methods. Comp Meth Appl Mech Engng 1990;83:143–98.
[38] Kikuchi N, Suzuki K. Structural optimization of a linearly elastic structure using the homogenization method. In: Rozvany G, editor. Shape and layout optimization in structural design, CISM Lecture Notes No. 325, Springer-Verlag, 1992.